Geomicrobiology Journal, 24:491–504, 2007

ISSN: 0149-0451 print / 1521-0529 online
DOI: 10.1080/01490450701572416

Taylor & Francis
Taylor & Francis Group

Mineralogical, Chemical and Biological Characterization of an Anaerobic Biofilm Collected from a Borehole in a Deep Gold Mine in South Africa

L. C. W. MacLean
Department of Earth Sciences, The University of Western Ontario, London, ON, Canada N6A 5B7

T. J. Pray and T. C. Onstott
Department of Geosciences, Princeton University, Princeton, NJ, USA 08544

E. L. Brodie and T. C. Hazen
Ecology Department, Earth Sciences Division, Lawrence Berkeley National Laboratory, Berkeley, CA, USA 94720

G. Southam
Department of Earth Sciences, The University of Western Ontario, London, ON, Canada N6A 5B7

A biofilm sample was collected from an anaerobic water and gas-flowing borehole, 1.474 km below land surface in the Evander Au mine, Republic of South Africa. The biofilm was 27 wt% ZnS, which was $\sim 2 \times 10^7$ times more concentrated than the dissolved Zn measured in the borehole water. X-Ray diffraction indicated that the Zn was present in the form of fine grained, 4.7 $\pm$ 0.9 nm particles with smaller amounts of pyrite (FeS_2). Scanning electron microscopy, coupled with energy-dispersive X-ray spectroscopy confirmed the identity of these minerals in the biofilm. Using transmission electron microscopy, the fine-grained ZnS minerals were found to coat the 1 μm-diameter rod-shaped bacteria that made up the primary substructure of the biofilm. The FeS_2 was present as framboids (spherical aggregates of 0.5–1 μm FeS_2 crystals) up to 10 μm in diameter and as large, 2–3 μm euhedral crystals that were not nucleated on the bacterial surfaces, but were found within the biofilm. Analyses of 16S rDNA utilizing clone libraries and a phylochip indicates that the ZnS rich biofilm is dominated by methanogens with a significant sulfate-reducing bacterial population and minor sulfide and CH_4-oxidizing chemolithotrophs. This biofilm community is sustained by sulfate, bicarbonate and H_2-bearing paleometeoric water.

Keywords deep subsurface, sulfate-reducing bacteria, ZnS, framboidal pyrite, community structure

Received 15 September 2006; accepted 30 May 2007.
Harmony Gold Mine, Inc. for providing access to the boreholes at Evander Mine. Evander geologists Colin Ralston, and Pete Roberts. Dr. Bob Cava of Princeton University and his student N. Rogado generously provided their lab's XRD and helped interpret the data. Funding was provided by grant EAR-9978267 from the National Science Foundation LExEn program to Onstott and Southam.
Address correspondence to L. C. W. MacLean, Center for Environmental Kinetics Analysis (CEKA), Pennsylvania State University, University Park, PA 16801, USA. E-mail: lmaclea@uwo.ca

INTRODUCTION

In natural environments, microorganisms commonly form complex biofilm communities that exhibit spatially unique geochemical behavior, significantly different than that produced by individual cells or found in the bulk solution (Little et al. 1997). These abrupt, localized chemical gradients and extracellular organic structures transform the biofilm–mineral interface into a highly heterogeneous environment (Geesey 2001). Detailed studies of the mineralogical, geochemical and biological properties of complex microbial communities are needed to better understand the dynamic influence that microbial communities can have on local biogeochemical cycles.

The existence of a diverse microbial ecosystem in the terrestrial deep subsurface has been well established (e.g., Fredrickson and Onstott 1996; Pedersen et al. 1997; Moser et al. 2003). Access to boreholes within the deep gold mines of South Africa has produced opportunities for the collection of microorganisms under indigenous subsurface conditions (Moser et al. 2003). For example, a flowing borehole that intersects a water-bearing fracture system can be viewed as an experimentally accessible extension of that fracture system. The high pressure, gaseous fracture water flushes out microbial contaminants introduced by the drilling process and by adjacent tunneling explosions; and if the environment of the borehole remains the same as that of the fracture system, indigenous microbes would colonize its interior surfaces.

If water and gas flow rates are sufficient, even a ceiling borehole angling up from a tunnel could remain anaerobic and free of any microbes utilizing the oxic/anoxic gradient where the borehole intersects the tunnel. Under these in situ conditions even high populations of microbes from surface contamination would have difficulty persisting once the original geochemical

conditions became re-established, favoring the indigenous microorganisms at the expense of the contaminating species (Pedersen et al. 1997; Moser et al. 2003).

Metal sulfides are found in a wide range of anaerobic environments and their formation has been attributed both to abiotic as well as biotic processes. Hydrothermal processes are attributed to sulfide formation at temperatures ~250°C (Trudinger et al. 1985) while biologically catalyzed sulfides are typically attributed to bacterial hydrogen sulfide production in low-temperature, anoxic environments (Berner 1970). Sulfate-reducing bacteria (SRB) use sulfate as a terminal electron acceptor releasing hydrogen sulfide as a metabolic by-product (Lovely and Klug 1983). The basic biogeochemical reactions mediated by dissimilatory sulfate-reducing bacteria (Tuttle et al. 1969) are:

$$2CH_2O + SO_4^{2-} \rightarrow H_2S + 2HCO_3^- \quad [1]$$

$$M^{2+} + H_2S \rightarrow MS + 2H^+ \quad [2]$$

The role of SRB in the formation of sulphide minerals is often considered to solely consist of sulphide formation (Rxn. 1), so much so that SRB are often replaced by H_2S to simplify experimental systems (Schoonen 2004). However, SRB exhibit an intimate association with the sulphide minerals they help form and recent studies have shown that SRB contribution can go beyond hydrogen sulfide formation (e.g., Donald and Southam, 1999; Druschel et al. 2002). For example, Donald and Southam (1999) demonstrated the ability of a mixed, anaerobic consortium of SRB to catalyze formation of pyrite via the formation of thin films of iron sulfides (FeS) on bacterial cell surfaces.

Iron sulphide is the most common metal sulphide attributed to sulphate reducing bacterial activity (Tuttle et al. 1969). Pyrite occurs as euhedral, e.g., cubic, or framboidal structural assemblages. Framboidal pyrite is dominant in modern anoxic environments and is preserved in ancient sedimentary rocks since the Proterozoic (Wilkin and Barnes 1997). Low temperature (<100°C) pyrite formation can occur by the reaction of FeS with oxidized sulfur compounds (e.g., Rxn. 3), which would occur in natural systems that encounter fluctuating redox boundaries (Berner 1969, 1970; Rickard 1975). It can also occur in anaerobic systems by the reaction of FeS with H_2S (Wilkin and Barnes 1997; Rickard 1997; Rickard and Luther 1997; Butler and Rickard 2000b; Rxn. 4) or of bacterially precipitated FeS with sulfur from the intracellular organic sulfur pool, presumably H_2S released from cysteine (Donald and Southam 1999).

$$FeS + S \rightarrow FeS_2 \quad [3]$$

$$FeS + H_2S \rightarrow FeS_2 + H_2 \quad [4]$$

In this study, we have characterized the geochemical and mineralogical structures of a sulfide-bearing biofilm sampled from deep inside an anaerobic borehole in the Evander gold mine, Republic of South Africa. The characterization of this biofilm provides insight into subsurface microbial mineralization processes and potentially the formation of low temperature sulfide ore deposits. It also provides clues as to the evolution of life on the early Earth, as well as lessons on how life might occur within other planets in our solar system.

EXPERIMENTAL PROCEDURES

Sample Site

The Evander mine is located 70 km east of Johannesburg, South Africa, within the Evander Basin. The Evander Basin is ~40 km long by 100 km wide and lies on the eastern edge of the larger Witwatersrand Basin. The basin's strata are comprised of a series of 2.9 Ga Au-bearing quartzite, conglomerate and shale beds, 2.7 Ga mafic volcanic units and 2.5 Ga carbonate deposits, all dissected by numerous 2.7 to 0.2 Ga dykes and sills and unconformably overlying a 3.5–3.0 Ga Archean basement (Tweedie 1981). A 30-year-old, 30 mm diameter borehole in the ceiling of a side cubby to the tunnel at 1.474 km depth at 2 shaft that projected upwards at a 45° angle for 25 meters and that intersected a fluid filled-fracture in the 2.7 Ga Footwall basalt sill was selected for this study.

The water and gas flow rates were between 100 to 125 mL min^{-1} and 100 to 150 mL min^{-1}, respectively. The temperature (30.9°C) and pH (pH 7.4) of the borehole water was measured using a digital thermometer (Fisher brand) and a Piccolo pH Meter (Hanna Instruments Inc.,Woonsocket, RI, USA), verified against litmus test strips. Oxidation/reduction potential (Eh = −50 mV) was measured with an Orion platinum electrode (Orion Research Inc., Beverly, MA, USA) and the instrument readout corrected according to Zobell (1946). The black biofilm that had presumably built up over the several-year lifespan of the borehole occupied a large fraction of the hole's volume.

Sampling Procedure

Three biofilm samples were collected 1 to 3 m, 3 to 6 m and 6 to 8 meters into the borehole using 15 mL falcon tubes fixed to an Al pole. Upon extraction from the borehole, each sample vessel was capped, stored on ice, and transferred to a field lab at the surface.

The biofilm sample was split under sterile conditions in an anaerobic glove bag and stored in individual cryotubes for further analysis. Samples for microscopy were fixed in $3\%_{(aq)}$ formaldehyde and refrigerated. Samples for DNA, elemental and X-ray diffraction studies were treated with 30% glycerol and stored at −20°C prior to being transported to Princeton, New Jersey.

Geochemical Analysis

The cation, trace metal and anion concentrations of the biofilm pore fluid were analyzed following the procedure of Onstott et al. (2006). The elemental composition of the black biofilm from the deepest sample was also measured by ICP-AES (Perkin Elmer). The mineralogical composition of the black

biofilm was determined by XRD analyses (Scintag PAD V). The mineral stability and reaction modeling of the biofilm under the measured geochemical conditions was performed using Geochemist's Workbench release 6.02 (Rockware, Inc., Golden, CO, USA; thermo.dat).

X-Ray Diffraction

A portion of the biofilm sample was thawed, rinsed with ethanol and dried over filter paper. The dried sample was ground up and analyzed with a Scintag PAD V X-ray diffractometer.

Scanning Electron Microscopy

A fraction of the biofilm sample was prepared for scanning electron microscopy (SEM) and energy dispersive X-ray spectroscopy (EDX) analysis. The sample was filtered through a 0.45 μm Millipore nylon filter, sequentially dehydrated with ethanol, and critically-point dried. To avoid charging, the sample was sputter-coated with a gold-palladium alloy and then examined with a LEO 1540XB FEG-SEM equipped with an EDX detector.

Transmission Electron Microscopy (TEM)

Biofilm samples for TEM were fixed with $2\%_{(aq)}$ glutaraldehyde, washed once using de-ionized H_2O, embedded in $2\%_{(aq)}$ (wt./vol.) low-melt agarose, sequentially dehydrated with ethanol and embedded in LR white resin (Fortin et al. 1995). Ultrathin-sections (70 nm) were cut using a Reichert Ultracut E ultramicrotome and placed on Formvar-carbon coated 200-mesh copper grids and viewed unstained in a Philips CM 10 TEM with EDX. Samples for high-resolution TEM were prepared as above but placed on holey-carbon 200-mesh copper grids and viewed in a JEOL2010F HRTEM. The HRTEM was also used to generated a Fourier transform (computer-based aggregate correcting for mineral orientation, i.e., rotation) Selected Area Electron Diffraction (SAED) pattern.

DNA Analysis

DNA was extracted from samples using the UltraClean Soil DNA Mega Prep kit (MoBio Laboratories Inc., Solana Beach, CA, USA) with shaking at 70°C and vortexing with beads. Small subunit rRNA genes (SSU rDNAs) were amplified using TaKaRa LA Taq polymerase (Panvera, Madison, WI, USA) using the provided buffers, dNTPs and reaction mixtures containing oligonucleotide primers at 0.4 μM and template at 50 ng/μL. For the 16S rDNA clone libraries, the forward primers 27f (*Eubacteria*-specific; Giovannoni 1991) and 8aF (*Archaea*-specific, Eder et al. 1999) were used with the universal reverse primer, 1492r (Lane 1991). Reliable amplification of archaeal rRNA genes required a nested reaction in which the product generated using primers 8aF and 1492r (Lane 1991) was used as the template for a second round of PCR with primers 109F (Lane 1991) and 958R (Pudry et al. 2002). All PCR amplification was carried out in a Stratagene Robocyler Gradient 96 (Stratagene, Cedar Creek, TX). The protocol began with an initial denaturation for 2 min at 95°C, followed by 35 cycles of 30 s at 95°C, 45 s at 54°C, and 1 minute 30 s at 72°C. The reaction was completed by a final extension at 72°C for 7 minutes. The DNA was purified, set into a clone library using a TOPO 10F' vector kit (Invitrogen, Carlsbad, CA), amplified using primers M13f and M13r, screened for unique clones by restriction fragment length polymorphism (RFLP) analysis using the enzymes, HAE III, for bacterial, and RSAI, for archaeal clones, and sequenced using primers M13f and M13r. Operational taxonomic units (OTU's) were defined following the approach of Gihring et al. (2006).

The sequences were visually evaluated for noise and meaningful length using Chromas (Technelysium Pty. Ltd., Tewantin, Queensland, Australia) and then matched with known sequences using the National Center for Biotechnology Information (NCBI) Blast search tool. Distance matrix trees were constructed for the bacterial and archaeal sequences and for selected sequences from NCBI using MegAlign (Lasergene). Bootstrap values were based on 1000 simulations.

PhyloChip Processing, Scanning, Probe Set Scoring and Normalization

16S rRNA gene amplification for PhyloChip analysis was carried out as described in Lin et al. (2006). The pooled PCR product (100 ng bacterial 16S rRNA, 13 ng archaeal 16S rRNA) was spiked with known concentrations of synthetic 16S rRNA gene fragments and non-16S rRNA gene fragments as internal standards for normalization with quantities ranging from 5.02×10^8 and 7.29×10^{10} molecules applied to the final hybridization mix. Target fragmentation, biotin labeling, PhyloChip hybridization, scanning and staining were as described by Brodie et al. (2006), while background subtraction, noise calculation, and detection and quantification criteria were essentially as previously reported (Brodie et al. 2006) with some minor exceptions. For a probe pair to be considered positive, the difference in intensity between the perfect match (PM) and mismatch (MM) probes must be at least 130 times the squared noise value (N). A taxon was considered present in the sample when 90% or more of its assigned probe pairs for its corresponding probe set were positive (positive fraction, pf $\geq$ 0.90).

Hybridization intensity (referred to as intensity) was calculated in arbitrary units (a.u.) for each probe set as the trimmed average (maximum and minimum values removed before averaging) of the PM minus MM intensity differences across the probe pairs in a given probe set. All intensities < 1 were shifted to 1 to avoid errors in subsequent logarithmic transformations. To account for scanning intensity variation from array to array, the intensities resulting from the internal standard probe sets were natural log transformed. Adjustment factors for each PhyloChip were calculated by fitting a linear model using the least-squares method. A PhyloChip's adjustment factor was subtracted from each probe set's ln(intensity).

TABLE 1
Elemental concentrations in the borehole water, the biofilm pore water and the dried biofilm, listed in order from highest to lowest concentration in the dried biofilm

Element	Borehole water M	Pore water M	Bulk biofilm mol/kg
Zn	5.35×10^{-7}	4.59×10^{-7}	2.79
S	8.20×10^{-3}*	2.97×10^{-3}**	2.69
Fe	$<1.79 \times 10^{-8}$	1.65×10^{-5}	1.34
Al	$<7.41 \times 10^{-9}$	n.a.	2.57×10^{-1}
Ni	$<1.70 \times 10^{-8}$	6.13×10^{-5}	1.58×10^{-1}
Si	3.64×10^{-4}	n.a.	1.44×10^{-1}
Ca	2.91×10^{-3}	2.73×10^{-3}	1.03×10^{-1}
Ba	1.75×10^{-6}	1.09×10^{-7}	5.49×10^{-2}
Co	1.70×10^{-8}	2.38×10^{-6}	4.45×10^{-2}
Na	1.67×10^{-2}	6.31×10^{-3}	3.51×10^{-2}
Cu	$<1.57 \times 10^{-8}$	2.36×10^{-7}	1.33×10^{-2}
As	$<6.67 \times 10^{-8}$	6.02×10^{-5}	1.13×10^{-2}
Sr	9.70×10^{-6}	8.50×10^{-6}	1.11×10^{-2}
Mn	4.20×10^{-5}	3.93×10^{-5}	8.03×10^{-3}
Li	3.31×10^{-5}	5.91×10^{-5}	2.10×10^{-3}
Mg	3.06×10^{-4}	9.05×10^{-5}	1.89×10^{-3}
Cr	$<1.61 \times 10^{-8}$	4.84×10^{-7}	1.20×10^{-3}
K	7.34×10^{-5}	5.45×10^{-5}	1.19×10^{-3}
U	1.51×10^{-7}	1.09×10^{-6}	5.05×10^{-4}

*Sulfate; **total sulfur.

RESULTS

Geochemistry and Mineralogy

Comparison of the elemental analyses for the borehole water flowing from the hole with that of the biofilm pore water (Table 1) reveal the Fe, Ni, Co, Cu, As, Cr and U concentrations are higher in the pore water, the Zn, Mn, Ca, Na, Sr, Li, K and Mg concentrations are similar between the pore and borehole water and the Ba concentration is lower in the pore water. The sulfate concentration in the pore water is less than that flowing out of the borehole. The most abundant elements by far in the biofilm are Zn (18 %wt.), S (9 %wt.) and Fe (7 %wt.). The apparent partitioning factor was calculated from the following relationship:

$$K = \{[X_b]\rho_b - \theta[X_w]\}/(1 - \theta) \quad [5]$$

where X_b = the concentration in the biofilm; X_w = the concentration in the pore water; ρ_b = the biofilm density (~1.5 kg L^{-1}); θ = the biofilm porosity (~50%). K was the highest for Zn, $\sim 2 \times 10^7$, followed by Ba, $\sim 2 \times 10^6$, Fe, $\sim 2 \times 10^5$, Co $\sim 6 \times 10^4$, and Ni $\sim 8 \times 10^3$.

At the observed pH and Eh of the borehole water, only witherite ($BaCO_3$) is slightly supersaturated (S.I. = 0.1) and sulfide minerals are undersaturated. Modeling the sulfate reduction reaction using acetate as the electron donor and the pore water chemistry and borehole pH and Eh as the initial conditions reveals that with only 5% conversion of sulfate to

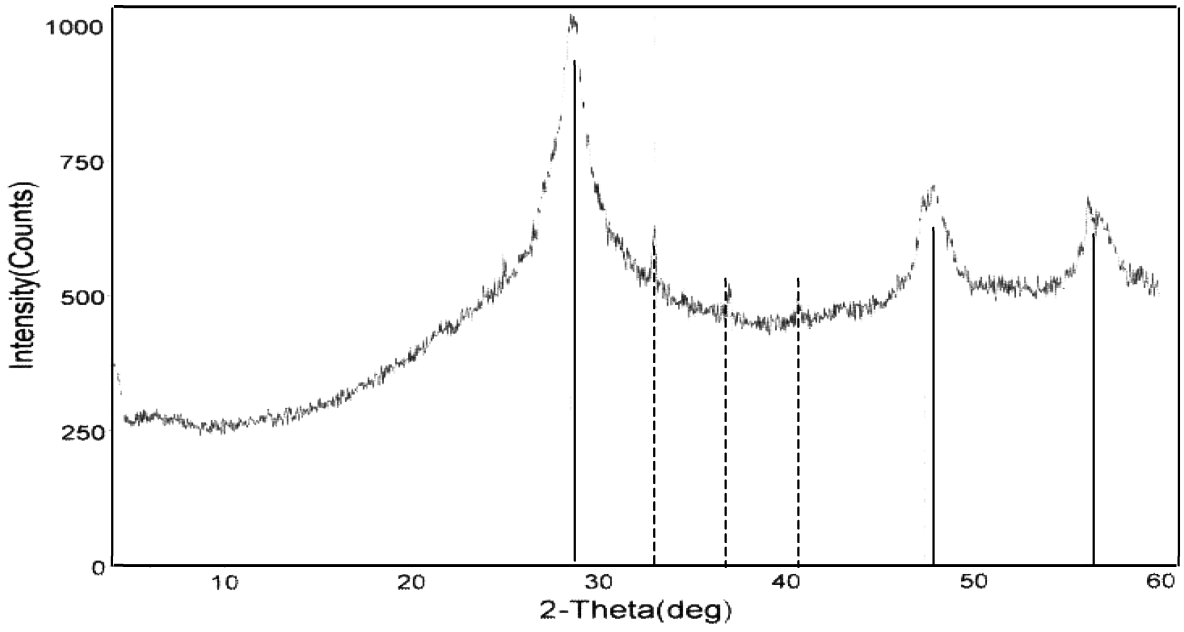

FIG. 1. X-Ray diffraction pattern obtained from a sample of dried biofilm. Solid lines correspond to broad peaks of ZnS and dashed lines to sharper pyrite (FeS_2) peaks.

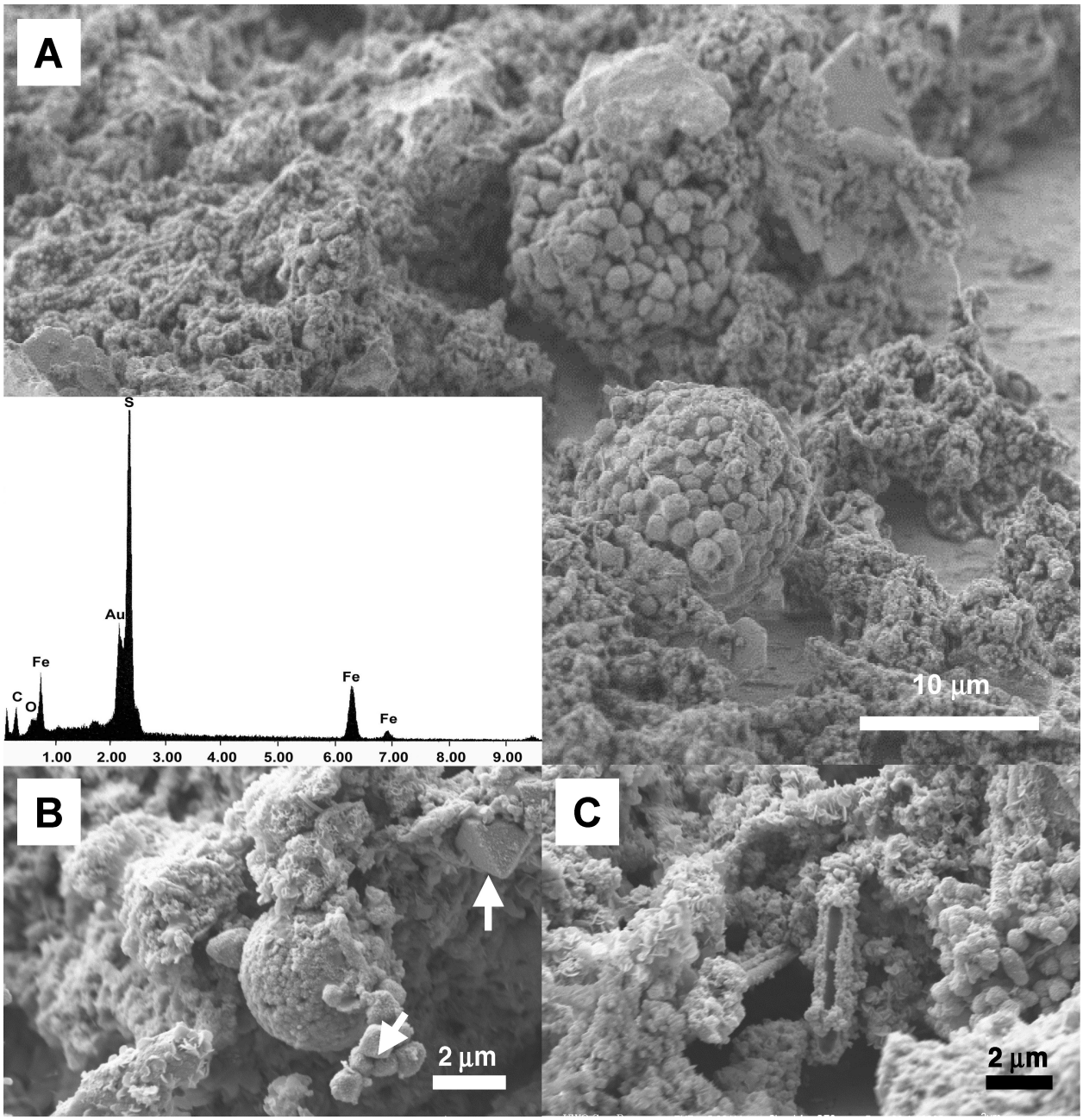

FIG. 2. (A) FEG-SEM micrograph of a portion of the mineralized biofilm. An organic matrix is observed throughout the structure. Framboidal pyrite is seen associated with the biofilm. (B) Pyrite is present as both smaller microcrystals that make up the framboid structure and larger euhedral crystals (white arrows). (C) Fossilized cells, mineralized by ZnS and FeS (EDX not shown).

sulfide, the Eh drops to -180 mV, the pH increases to 7.6 and the precipitation of pyrite, sphalerite, vaesite, chalcopyrite and covellite occurs. The precipitation of carbonates is also predicted to occur.

X-ray diffraction (XRD) revealed large, broad ZnS peaks and small but sharp FeS_2 peaks indicating that FeS_2 is less abundant than ZnS, but that its crystal sizes are larger than that of ZnS (Figure 1). The particle size was estimated using the Scherrer formula (Wilson 1963; Rxn. 6):

$$t = K\lambda/\beta\cos\theta \quad [6]$$

where t is the crystal size, K is a constant dependent on crystallite shape (0.9) , λ is the wavelength for Cu-Kα radiation (1.54 Å), β is the full width at half maximum and θ is from the 2θ of the maximum intensity peak in the XRD pattern (29°). Based on

this formula, the size of the ZnS mineral grains were calculated to be 4.7 ± 0.9 nm in size.

Scanning Electron Microscopy

Examination of the biofilm using field emission gun scanning electron microscopy (FEG-SEM) demonstrated that the "biofilm" consisted primarily of nanocrystalline ZnS (Figure 2A; EDX data not shown) and lesser amounts of framboidal (Figures 2A and B) and euhedral pyrite (Figure 2B). In some cases ZnS 'casts' of rod shaped bacteria could also be observed (Figure 2C). Overall the biofilm also possessed sub-cellular, filamentous, organic structures, which were loosely coated by metal sulfides. Interlocking 5 μm size plates of barite and 1 × 20 μm fibers of gypsum were also present, but no carbonate phases were detected.

Transmission Electron Microscopy

The TEM micrograph in Figure 3 represents a cross-section of the biofilm. The outline of fossilized microorganisms can be clearly distinguished throughout the biofilm structure. EDX analysis of the fossilized structures and the surrounding matrix reveals a dominant ZnS mineralogy that confirms the XRD analysis. HRTEM studies revealed the ZnS coating was composed of individual nanoparticles aggregated together with an average diameter of ∼5 nm (Figure 4A and 4B). The Fourier transform SAED pattern of the aggregated crystals demonstrated their crystallinity, but appears to be a composite of cubic sphalerite and hexagonal wurtzite (Figure 4C).

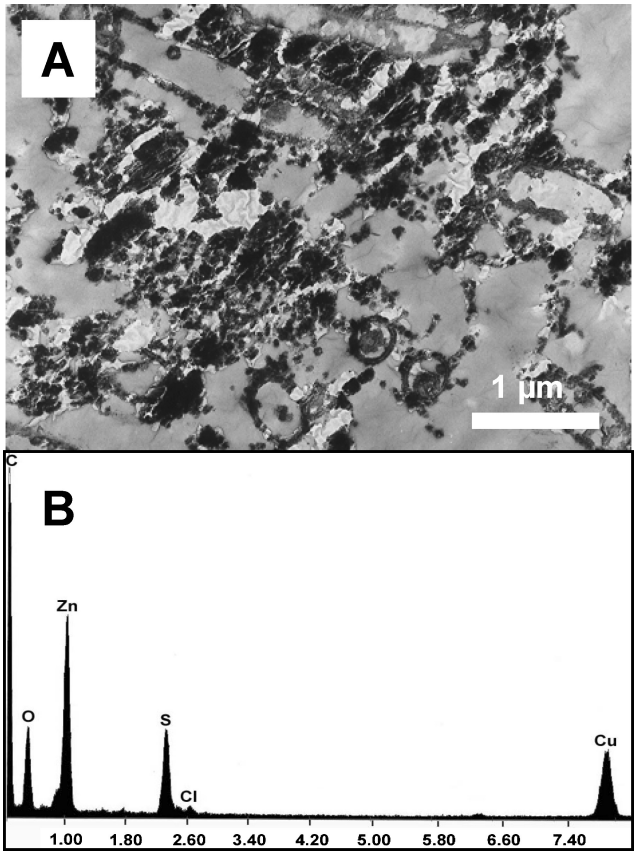

FIG. 3. Ultrathin sectionTEM micrograph of the mineralized biofilm. Fossilized microbes can be viewed throughout. (B) EDX spectrum of the mineralized structures showing ZnS precipitation is predominant throughout the biofilm. The Cu signal is from the Cu TEM grid.

Community Structure

Thirty-six OTUs were identified from 45 bacterial clones and 16 OTU's were identified from the 39 archaeal clones (Table 2). Twenty-seven of the 36 bacterial OTU's are 86 to 99% similar to clones or bacterial isolates from anaerobic psychrophilic to thermophilic environments. Seven of the bacterial clones are 91 to 95% similar to sulfate or S°-reducing bacterial species belonging to the δ *Proteobacteria*, *Firmicutes* and *Nitrospirae* phyla and of these, one of the *Firmicutes* clones was 91% similar to the *Desulfosporosinus* species 44a-T3a recovered from the mine site described by Labrenz et al. (2000).

TJB45 was 91.8% similar to *Desulfacinum subterranium,* a thermophilic SRB found in a high-temperature oil field, that grows optimally at 60°C, and can use H_2 as an electron donor with only CO_2 as a carbon source (Rozanova et al. 2001). Nine of the bacterial OTU's are 89 to 99% similar to uncultured clones reported for other S. African Au mines (Table 2). One bacterial OTU belonging to the *Spirochaetes* is 99% similar to Fe(III) reducing and obligate anaerobic fermenter SA-10 isolated from Merriespruit Au mine (Bonin 2005). Of the 9 remaining OTU's not similar to clones or isolates from anaerobic environments, 3 are 95 to 99% similar to sulfide or S°-oxidizing β *Proteobacteria* isolates, 2 are 94 to 98% similar to a methanotrophic γ *Proteobacteria* isolate, and the remainder are similar to miscellaneous *Proteobacteria,* or *Gemmatimonadetes* isolates or clones (Table 2).

The archaeal clone library is dominated by 1 Euryarcheota OTU, TJA29, which is 91% similar to a clone Papm3A44 extracted from a Mariana trough hydrothermal vent (Table 2). Of the remaining 15 OTUs, 5 are 92 to 93% similar to the same Mariana trough clone, 3 are 90 to 92% similar to Euryarcheota clones reported from a deep sea sulfide vent (Shrenk et al. 2003), 4 are 93 to 98% similar to member of an anaerobic CH_4 oxidizing consortium (Raghoebarsing et al. 2006), 2 are 93% to 95% similar to petroleum-contaminated soil (Kasai et al. 2005) and 1 is 98% similar to a Creanarcheota clone derived from subseafloor sediments from the sea of Okhotsk (Inagaki et al. 2003) (Table 2). Thirteen of the 16 OTUs are similar to clones recovered from other S. African Au mines, but none of them fall within the SAGMEG or SAGMCG groups (Gihring et al. 2006).

Ten of the OTUs are 90 to 97% similar to a Euryarcheota clone reported for a borehole from Merriespruit Au mine, where the CH_4 has been classified as methanogenic by its isotopic signature (Sherwood Lollar et al. 2006) and from which a methanogen has been isolated (Bonin 2005). Based

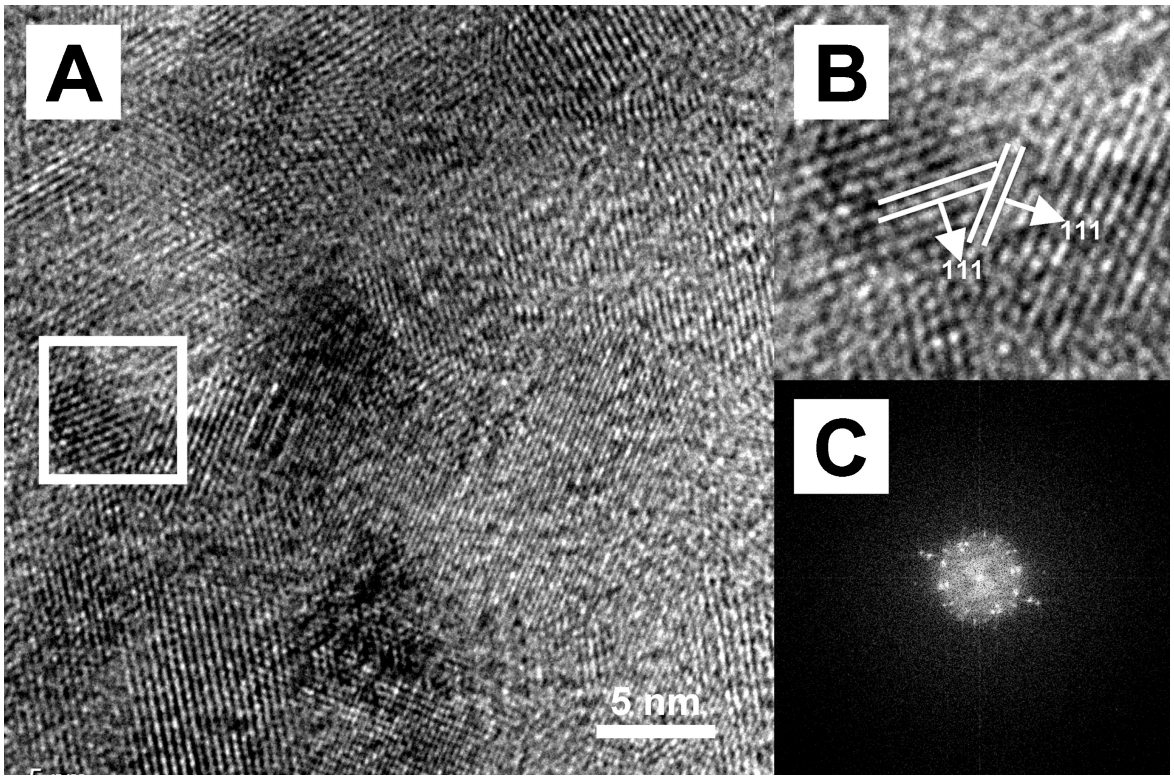

FIG. 4. HRTEM images of the ZnS nanoparticles. (A) Randomly oriented lattice fringes are visible. (B) Mis-orientation at the Interface of two nanocrystals. (C) Fourier transform diffraction pattern of B, demonstrating the crystallinity of the nanoparticles.

on Schao1 statistics (Chao 1984; 109 for the bacteria and 58 for the archaea), neither clone library sampled the complete diversity present in the biofilm; therefore, we analyzed the biofilm samples using the phylochip.

PhyloChip Analysis of Microbial Relative Abundance in Biofilm Scrapings with Increasing Distance into the Fracture Borehole

Hierarchical clustering of PhyloChip intensities was used to identify the response of bacterial and archaeal taxa with depth into the fracture borehole (Figure 5). Bacterial richness (number of PhyloChip taxa above 0.90 probe positive fraction) peaked 6 m into the borehole with 1,596 bacterial taxa compared with1,434 for the outermost (3 m) biofilm sample, while bacterial richness was lowest 8 m into the borehole (982 taxa). The same trend was noted for archaeal richness with 31, 21 and 22 archaeal taxa detected in the 6, 3 and 8 m biofilms, respectively. The difference in archaeal diversity was entirely due to increased diversity within the Euryarchaeota in the 6 m sample. Within the bacteria, β proteobacterial richness decreased with depth into the borehole (148, 137, 77 taxa for 3, 6 and 8 m samples respectively), while δ proteobacterial richness was maximal in the 6 m biofilm scraping (104, 116, 89 taxa).

The 16S rDNA phylochip revealed that the subsurface (deeper, 8 m) microbial community is dominated by Archaea, especially methanogens, but with a diverse bacterial community that mirrors the clone library and comprised of *Firmicutes, δ Proteobacteria* and*Nitrospirae* sulfate reducers, *γ Proteobacteria* S oxidizers, methanotrophic, NH_4^+ oxidizing and N_2 fixing *Proteobacteria* (Figure 5). The phylochip analyses of the biofilm samples collected at 1 to 3 meters and 3 to 6 meters into the borehole reveal a transition from a community dominated by Bacteria to one with equal proportions of both to the 6 to 9 meter samples in which the Archaea are clearly dominant (Figure 5). Methanotrophs were more abundant in the shallowest biofilm sample. The biofilm community at intermediate depths was comprised of the greatest bacterial diversity with both aerobic and anaerobic members reflecting the transition from oxic to anoxic borehole environments.

DISCUSSION

The results of our investigation are similar to that of Labrenz et al. (2000) who reported a Zn biofilm concentration 10^6 times that of the measured groundwater versus the 2×10^7 times reported in this study, suggesting that the biosphere can readily produce economically viable enrichments of Zn (Druschel et al. 2002) . Both aqueous systems were at circumneutral pH and had similar Fe ($\sim$ 17 μM) and S (3 to 8 mM) concentrations. Labrenz et al. (2000), however, found no FeS_2 in their biofilm.

TABLE 2
Bacteria and archaeal BLAST match

OTU	# of clones	Group/phylum	% similar	Closest relative	Physiology/ Environment	Assn. No.	Ref#
TJB14	1	αProteobacteria	93.1	Bacterium Ellin328	Soil	AF498710	1
TJB51	1	βProteobacteria	99.6	uncult. bac. clone	Deep groundwater	AB179676	2
			89.4	uncult. bac. clone SAJJ44	Ev818 H5 core parings	DQ337045	3
TJB48	1	βProteobacteria	99.2	uncult. bac. clone TSAU03	Microcosm	AB186833	4
			96.6	*Zoogloea oryzae*	N_2-fixing rice paddy bacterium	AB201044	5
TJB17	1	βProteobacteria	98.5	uncult. bac. clone #12	Be23FW031301fr acture water	DQ088746	6
			98.0	*Thiobacillus denitrificans*	Anerobic S° oxidizer	CP000116	7
TJB13	1	βProteobacteria	99.2	*Thiomonas sp.*	S° oxidizing bacteria	AY438665	8
TJB2	1	βroteobacteria	99.0	uncult. bac. clone	Ev818 mining water	DQ337096	3
			95.0	*Thiobacillus plumbophilus*	Galena and H_2 chemolithotroph	AJ316618	9
TJB36	1	γProteobacteria	98.2	*Methylocaldum gracile*	CH_4 oxidizer	U89298	10
TJB3	1	γProteobacteria	94.0	*Methylococcus capsulatus*	Methanotrophic bacteria	AJ563935	11
			94.6	uncult. bac clone #36	Be16FW031601 h1-fracture water	DQ088732	6
TJB55	1	δProteobacteria	92.4	*Desulfobulbus propionicus*	Sulfate-reducing fluidized-bed reactor	AY548789	37
TJB49	1	δProteobacteria	93.0	uncult. bac clone BSB16-364m	Black Sea oxic/anoxic chemocline	AY360500	12
			94.8	*Desulfobacteraceae*	Sulfate-reducing lake	AJ582703	13
TJB45	1	δProteobacteria	97.0	uncult. bac. clone RPS-IB3	CH_4 generating fuel cell	AB288574	14
			91.8	*Desulfacinum subterranium*	Thermophilic sulfate reducer	AF385080	15
TJB33	2	δProteobacteria	89.1	*Anaeromyxobacter dehalogens*	Aryl-halorespiring facultative anaerobe	AF382400	16
TJB11	1	δProteobacteria	89.5	uncult. bac. clone	Hypersaline mat	DQ331004	17
TJB58	1	Chlorobi	95.2	uncult. bac. clone SAJJ39	Ev818 H5 core parings	DQ337042	3
			85.7	anammox bacteria A3	Anaerobic NH_4^+ oxidizer	AM056028	18
TJB37	1	Chlorobi	94.3	uncult. bac. clone 655939	U contaminated aquifer	DQ404811	19
			93.5	uncult. bac. clone	Sulfide-rich Dr546bh1 biofilm	AF546951	20
TJB54	1	Chloroflexi	96.0	uncult. bac. clone AKYG408	Whale fall	AY921833	21
TJB41	1	Chloroflexi	96.0	uncult. bac. clone	Sulfate-reducing anaerobic reactor	AB195873	22
TJB40	2	Chloroflexi	95.4	uncult. bac. clone	Thermophilic methanogenic sludge	AB109437	23
TJB39	1	Chloroflexi	95.8	uncult. bac. clone	Cellulose fed microbial fuel cell	AB286297	24

TJB35	1	Chloroflexi	93.4	uncult. bac. clone AKYG1569	Whale fall	AY921906	21
TJB34	1	Chloroflexi	92.7	uncult. bac. clone ODP1227B19.08	Deep sea sediments	AB177058	25
TJB22	3	Chloroflexi	95.5	uncult. bac. clone #TTA B60	Thermophilic anaerobic reactor	AY297975	26
TJB16	1	Chloroflexi	99.4	uncult. bac. clone	Sulfate-reducing anaerobic reactor	AB195873	22
TJB29	1	Gemmatimonadetes	95.3	uncult. bac. clone BF23	Oxidation reactor	DQ839330	27
			87.6	*Gemmatimonas aurantiaca*	Polyphoshate accumulating bacterium	AB072735	28
TJB56	1	Firmicutes	92.3	*Desulfitobacterium metallireducens*	Sulfate-reducing bacterium	AF297871	29
			90.1	Desulfitobacterium RPf35Ei	Sulfate-reducing fluidized-bed reactor	AY548779	30
TJB42	1	Firmicutes	93.2	uncult. bac. clone B24	Deep sea vent biofilm	AB260067	31
			96.0	uncult. bac. clone TTMF167	TT104 borehole	AY741688	32
TJB28	2	Firmicutes	94.3	uncult. bac. clone TIBH08	thermophilic anaerobic waste reactor	DQ887957	33
TJB9	1	Firmicutes	90.0	uncult. bac. clone	Gas hydrate mound sediments	AY211735	34
TJB1	1	Firmicutes	91.0	*Desulfosporosinus sp. 44a-T3a*	Sulfide rich mine biofilm	AY082482	35
			92.0	Desulfitobacterium sp. RPf35Ei	Sulfate-reducing fluidized-bed reactor	AY548779	30
TJB50	2	Nitrospirae	95.6	uncult. bac. clone 34	Be325FW032701 h1 fracture water	DQ088762	6
			91.6	*Thermodesulfovibrio spec. nov.*	Thermophilic sulfate reducer	EF081294	36
TJB4	3	Nitrospirae	98.1	uncult. bac. clone	Ev818 Mining water	DQ337083	3
TJB38	2	OP11	90.7	uncult. bac. clone	Antarctic shelf sediment	AF424454	37
TJB46	1	Spirochaetes	98.6	SA-10	Mesophilic IRB and fermenter	AY695841	38
TJB20	1	Verrucomicrobia	96.4	uncult. bac. clone #147	Acidic peat bog	AM162461	39
			96.4	uncult. bac. clone #176T36	Anaerobic fresh water sediments	DQ110052	40
TJB19	1	unclassified	85.9	uncult. bac. clone LCFA B10	Mesophilic methanogenic consortium	AB244317	41
TJB6	1	unclassified	96.2	uncult. bac clone #44	Anoxic lake sediment	AJ543758	42
No. of Clones	45						
No. of OTU's	36						
SChao1	109						
TJA3	1	Euryarchaeota	91.3	uncult. arch. clone FZ2bA167	Deep sea sulfide vent	AY166028	43
TJA24	1		92.6	uncult. arch. clone Papm3A44	Mariana Trough hydrothermal vent	AB213099	46
			91.2	uncult. arch. clone 34	Ms149 h1 062003-fracture water	DQ354739	3
TJA30	1		92.8	uncult. arch. clone Papm3A44	Mariana Trough hydrothermal vent	AB213099	46
			91.1	uncult. arch. clone 34	Ms149 h1 062003-fracture water	DQ354739	3
TJA54	3		91.1	uncult. arch. clone a25	Ev811-0305-fracture water	DQ088712	3
			90.2	uncult. arch. clone FZ2bA48	deep sea sulfide vent	AY166015	43

(Continued on next page)

TABLE 2
Bacteria and archaeal BLAST match (Continued)

OTU	# of clones	Group/phylum	% similar	Closest relative	Physiology/ Environment	Assn. No.	Ref#
TJA11	1		92.7	uncult. arch. clone Papm3A44	Mariana Trough hydrothermal vent	AB213099	46
			91.0	uncult. arch. clone 34	Ms149 h1 062003-fracture water	DQ354739	3
TJA12	1		91.9	uncult. arch. clone FZ1aA21	deep sea sulfide vent	AY165982	43
TJA13	1		92.1	uncult. arch. clone Papm3A44	Mariana Trough hydrothermal vent	AB213099	46
			91.0	uncult. arch. clone 34	Ms149 h1 062003-fracture water	DQ354739	3
TJA42	1		91.7	uncult. arch. clone Papm3A44	Mariana Trough hydrothermal vent	AB213099	46
			89.9	uncult. arch. clone 34	Ms149 h1 062003-fracture water	DQ354739	3
TJA29	19		91.1	uncult. arch. clone Papm3A44	Mariana Trough hydrothermal vent	AB213099	46
			90.6	uncult. arch. clone 34	Ms149 h1 062003-fracture water	DQ354739	3
TJA5	2	Unclassified	93.0	uncult. arch. clone D-ARCH	anaerobic CH_4 oxidation & denitrification	DQ369741	45
			95.7	uncult. arch. clone 32	Ms149 h1 062003-fracture water	DQ354743	3
TJA10, TJA46	2	Unclassified	97.4	uncult. arch. clone D-ARCH	anaerobic CH_4 oxidation & denitrification	DQ369741	45
			97.3	uncult. arch. clone 32	Ms149 h1 062003-fracture water	DQ354743	3
TJA25	3	Unclassified	97.8	uncult. arch. clone D-ARCH	anaerobic CH_4 oxidation & denitrification	DQ369741	45
			97.4	uncult. arch. clone 32	Ms149 h1 062003-fracture water	DQ354743	3
TJA34	1	Unclassified	95.4	uncult. arch. clone ASC26	petroleum contaminated soil	AB161329	47
			95.5	uncult. arch. clone 32	Ms149 h1 062003-fracture water	DQ354743	3
TJA44	1	Unclassified	93.7	uncult. arch. clone D-ARCH	anaerobic CH_4 oxidation & denitrification	DQ369741	45
			94.5	uncult. arch. clone SAP144	Ev818 mining water	DQ337108	3
TJA4	1	Crenarcheota	97.6	uncult. arch. clone OHKA4.59	Subseafloor sediments	AB094541	44
TJA32	1	Unclassified	88.3	uncult. arch. clone a15	EV914-0228-containment dam water	AB161349	47
			92.7	uncult. arch. clone ASN17	petroleum contaminated soil	DQ088718	3
No. of clones	39						
No. of OTU's	16						
SChao 1	35						

Ref. No. 1. Sait et al. 2002; 2. Miyoshi et al. 2005; 3. Gihring et al. 2006; 4. Yoshida et al. 2005; 5. Xie and Yokota 2006; 6. Lin et al. 2006; 7. Beller et al. 2006; 8. Chen et al. 2004a; 9. Drobner et al. 1992; 10. Bodrossy et al. 1997; 11. Dedysh et al. 2004; 12. Vetriani et al. 2003; 13. Stubner (NCBI); 14. Ishii et al. (NCBI); 15. Rozanova et al. 2001; 16. Sanford et al. 2002; 17. Ley et al. 2006; 18. Jia and Xu (NCBI); 19. Abulencia et al. 2006; 20. Moser et al. 2003; 21. Tringe et al. 2005; 22. Kim et al. (NCBI); 23. Yamada et al. 2005; 24. Ishii et al. (NCBI); 25. Inagaki et al. 2006; 26. Chen et al. 2004b; 27. Lin et al. (NCBI); 28. Zhang et al. 2003; 29. Finneran et al. 2002; 30. Kaksonen et al. 2004; 31. Nakagawa et al. 2006; 32. Milleson and Kieft (NCBI); 33. Li et al. (NCBI); 34. Mills et al. 2003; 35. Labrenz and Banfield (NCBI); 36. Haouari et al. (NCBI); 37. Bowman and McCuaig, 2003; 38. Bonin, 2005; 39. Dedysh et al. 2006; 40. Weber et al. 2006; 41. Shigematsu et al. 2006; 42. Bottinelli et al. (NCBI); 43. Schrenk et al. 2003; 44. Inagaki et al. 2003; 45. Raghoebarsing et al. 2006; 46. Kato et al. (NCBI); 47. Kasai et al. 2005.

Each sequence, labeled according to which of the original cloned PCR products and the name of the closest reference organism with percent similarity to the sequence.

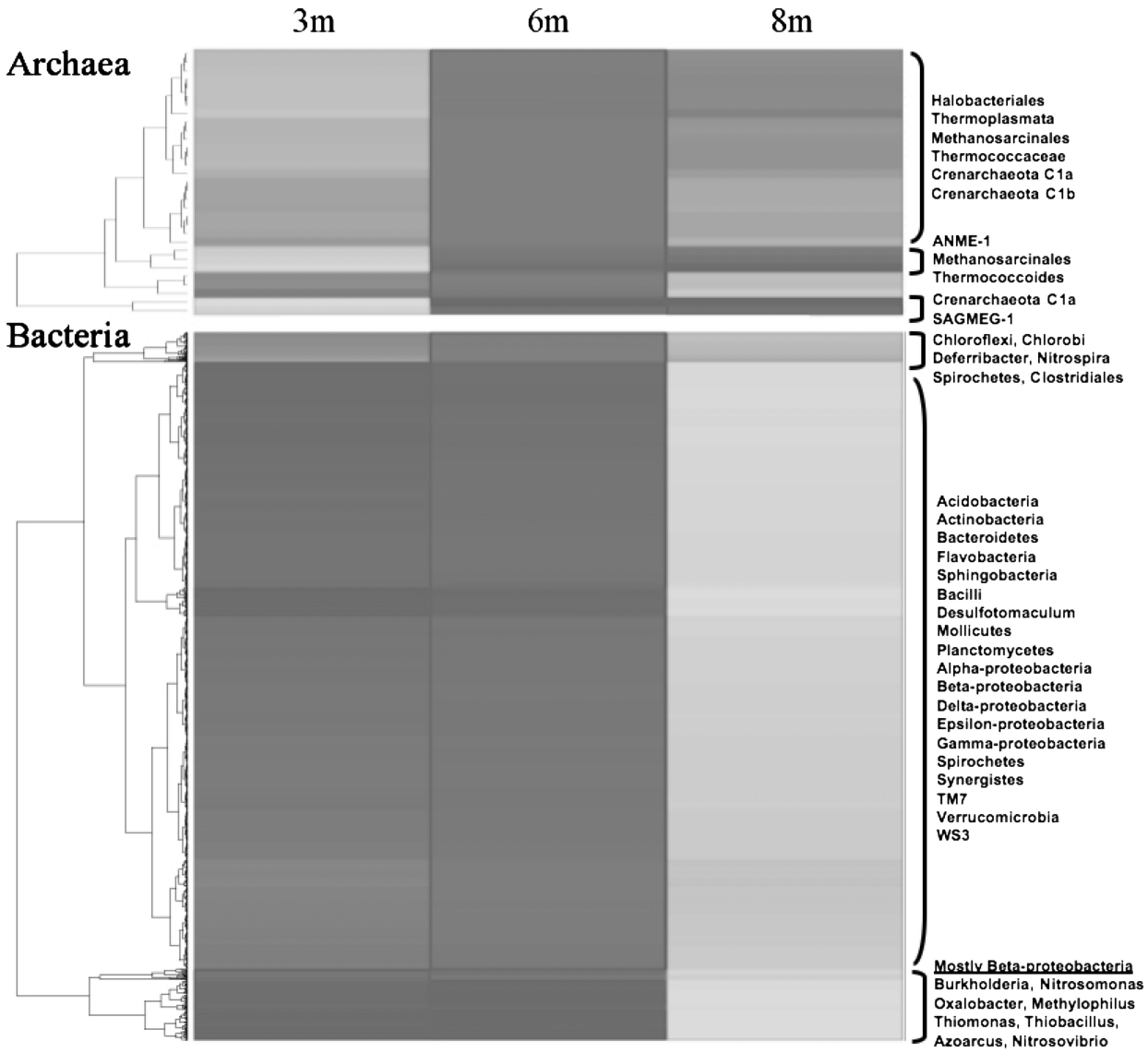

FIG. 5. A heat-plot of the 16S rDNA PhyloChip results (see Brodie et al. 2006) demonstrating a transition from a community dominated by Bacteria (3 m label), to one with equal proportions of both (6 m), to one in which the Archaea are clearly dominant (8 m).

We attribute the presence of pyrite in our study to the lower concentration of Zn in the borehole water. Labrenz et al. (2000) and Druschel et al. (2002) presented a geochemical model, based on solution chemistry and kinetic restraints, which predicts that single mineral deposits would indicate formation under conditions where metals are re-supplied at rates that are higher than rates of sulfide replenishment.

Precipitation of one metal will take up sulfide faster than can be produced by bacterial sulfate reduction, preventing the saturation of a second metal sulfide. After depletion of the first metal, sulfide can then accumulate enough for a second metal sulfide phase to emerge. In their model, Labrenz et al. (2000) and Druschel et al. (2002) predicted that the sequence of metal sulfide mineralization would be CuS, followed by CdS, then ZnS, PbS, and finally FeS. In our system, the presence of a second metal sulfide, pyrite, is probably due to Zn depletion, which allowed the precipitation of a second sulfide phase.

Reaction modeling of the borehole water confirms that both ZnS and FeS_2 will precipitate within our system if these metals are continuously supplied. Isotopic data indicate that the source of the borehole water is the 37-kyr-old ground water from the overlying Karoo formation, which contains only 0.2 μM Zn versus 70 μM of Fe (Onstott et al. 2006). Since the borehole water emanates from fractures deeper in the borehole than we sampled, the Zn may be preferentially removed and concentrated in deeper biofilms leaving Fe to migrate further down the borehole biofilm where it precipitates as a sulfide. Reaction modeling also predicts that siderite will precipitate.

The fact that it wasn't observed could mean that the HCO_3^- concentration within the microenvironment of the biofilm is much lower than in the borehole fluid possibly because it is being consumed by autotrophic methanogens.

Images obtained with FEG-SEM and TEM showed that rod-shaped bacteria within the biofilm were coated with ZnS (Figures 2 and 3) and confirm the XRD measurements in which the highest peaks in the XRD spectrum corresponded to ZnS (Figure 1). The size of the ZnS particles calculated by peak broadening analysis was corroborated by the HRTEM investigation (Figure 4). The random arrangement of the ZnS nanoparticles, i.e., presenting different crystal face orientations (Figure 4A) and possessing inter-planar dislocations (Figure 4B) demonstrates that they are not crystallographically parallel. This suggests that the individual nanocrystals had nucleated and aggregated at or near a heterogeneous surface(s). Flocculation of nanoparticles at a surface has been proposed to prevent the coherent attachment of nanocrystals usually observed during nanoparticle aggregation in solution (Banfield et al. 2000). Briefly, nanoparticles that have formed in solution away from a surface will have achieved a coherent particle-particle interface through freedom or orientation in solution, leading to eventual coarsening.

Nanoparticles that have nucleated side by side and flocculated at a surface, however, would tend to have been confined in their ability to rotate and achieve a coherent particle-particle interface (imperfect orientation) and show evidence of boundary dislocations (Figure 4B) (Penn and Banfield 1998; Banfield et al. 2000). Due to the lack of crystal coarsening under these conditions, it has been suggested that microbial cell morphologies may be preserved in the mineral record in the form of textural differences between the smaller aggregated nanoparticles and the surrounding mineral matrix (Banfield et al. 2000, 2001; Cady et al. 2003). A mineralogical biosignature in combination with biomarkers of a chemical nature (e.g., Benzerara et al. 2006; c.f. Figures 1 and 4) may provide the type of unambiguous biomarker needed in the search for life in ancient materials on Earth and on other planets, i.e., Mars.

The presence of both framboidal and euhedral pyrite within the biofilm is interesting because it suggests that the formation of pyrite occurred under two different sets of chemical conditions. A pyrite framboid is a spherical aggregate of 0.5–1 μm FeS_2 crystals (Wilkin and Barnes 1997). Butler and Rickard (2000a) suggested that pyrite supersaturation can increase with small increases in Eh of a system. They presented experimental results that showed pyrite framboids formed in weakly acidic to weakly alkaline conditions under slightly oxic conditions (Eh $>$ –250 mV). The rate of pyrite nucleation, therefore, is higher than the rate of crystal growth and the result is multiple pyrite microcrystals of the same size with limited microcrystal growth. In contrast, euhedral pyrite was observed to form under lower supersaturation conditions at low Eh (–400 mV), when rates of crystal growth are higher than rates of nucleation (Butler and Rickard 2000a). The presence of both forms of pyrite in this system suggests that microenvironments possessing a range of anaerobic Eh conditions must have existed with this biofilm. This range of Eh is consistent with the geochemical model and the community diversity.

Analysis of relative abundance patterns (Figure 5) demonstrated that archaeal abundance was typically higher in the 6 m sample with the exception of a taxa from the South African Gold Mine Euryarchaeote Group 1 (SAGMEG-1) and a C1a group Crenarchaeote. However, present in the biofilms at all locations were acetoclastic methanogens of the genus *Methanosarcina*. Interestingly the biofilms also contained members of the anaerobic methane oxidizing archaeal group ANME-1. The bacterial community appeared to be stratified with depth from the borehole opening with aerobic beta-proteobacteria being more abundant at 3m but declining in abundance further into the borehole.

These taxa included known methane, sulfide and ammonia oxidizers, suggesting the presence of molecular oxygen. The intermediate 6 m biofilm samples showed the greatest diversity of bacteria detected and contained many metal-reducing taxa including sulfate and iron reducers and nitrogen fixing bacteria. The high diversity of the bacteria found within this "ecosystem" appears to reflect both indigenous microbial populations and microorganisms that have been reported in the mining water and may represent contaminants from the drilling process or mine air. When the borehole was drilled, the fractures would have been initially contaminated with aerobic and aerotolerant microorganisms, some of which include sulfide-oxidizing chemolithotrophs and methanotrophs (Onstott et al. 2003) surviving on the reduced metals, H_2 and hydrocarbons emanating into the borehole from the fractures.

But as the CH_4 generated by methanogens within the fractures begins to displace the mine air in the borehole, the borehole environment and the biofilm within the borehole becomes progressively more anaerobic. The sulfate-reducing bacteria and methanogens supplant the chemolithotrophs and methanotrophs in the biofilm as the metal rich biofilm progressively marches its way down the borehole towards the opening. What is clearly evident from examination of this borehole is that in a space of several years sulfate-reducing bacteria encountering sub μM levels of dissolved Zn deposited a ZnS rich biofilm that if continued over geologic time would produce an economic deposit.

REFERENCES

Abulencia CB, Wyborski DL, Garcia JA, Podar M, Chen W, Chang SH, Chang HW, Watson D, Brodie EL, Hazen TC, Keller M. 2006. Environmental whole-genome amplification to access microbial populations in contaminated sediments. Appl. Environ Microbiol 72:3291–3301.

Banfield JF, Welch SA, Zhang H, Ebert TT, Penn RL. 2000. Aggregation-based crystal growth and microstructure development in natural iron oxyhydroxide biomineralization products. Science 289:751–754.

Banfield JF, Moreau JW, Chan CS, Welch SA, Little B. 2001. Mineralogical biosignatures and the search for life on Mars. Astrobiol 1:447–467.

Beller HR, Chain PSG, Letain TE, Chakicherla A, Latimer FW, Richardson PM, Coleman MA, Wood AP, Kelly DP. 2006. The genome sequence

of the obligately chemolithoautotrophic, facultatively anaerobic bacterium *Thiobacillus denitrificans*. J Bacteriol 188:1473–1488.

Benzerara K, Menguy N, Lopez-Garcia P, Yoon TH, Kazmierczak J, Tyliszczak T, Guyot F, Brown GE. 2006. Nanoscale detection of organic signatures in carbonate microbialites. Proc Natl Acad Sci USA 103:9440–9445.

Berner RA. 1969. The synthesis of frambiodal pyrite. Econ Geol 64:383–384.

Berner RA. 1970, Sedimentary pyrite formation. Amer J Sci 268:1–23.

Bodrossy L, Holmes EM, Holmes AJ, Kovacs KL, Murrell JC. 1997. Analysis of 16S rRNA and methane monooxygenase gene sequences reveals a novel group of thermotolerant and thermophilic methanotrophs, *Methylocaldum* gen. nov. Arch. Microbiol 168:493–503.

Bonin AS. 2005. Deep subsurface microbiology of the south African gold mines. Ph.D. Dissertation, Portland State University. 116 pp.

Bowman JP, McCuaig RD. 2003. Biodiversity, community structural shifts, and biogeography of prokaryotes within Antarctic Continental Shelf sediment Appl Environ Microbiol 69:2463–2483.

Brodie EL, DeSantis TZ, Joyner DC, Baek SM, Larsen JT, Andersen GL, Hazen TC, Richardson PM, Herman DJ, Tokunaga TK, Wan JM, Firestone MK. 2006. Application of a high-density oligonucleotide microarray approach to study bacterial population dynamics during uranium reduction and reoxidation. Appl Environ Microbiol 72:6288–6298.

Butler IB, Rickard DT. 2000a. The origin of framboids. Lithos 3:269–293.

Butler IB, Rickard D. 2000b. Framboidal pyrite formation via the oxidation of iron (II) monosulphide by hydrogen sulphide. Geochim Cosmochim Acta 64:2665–2672.

Cady SL, Farmer JD, Grotzinger JP, Schopf JW, Steele A. 2003. Morphological biosignatures and the search for life on Mars. Astrobiol 3:351–368.

Chao A. 1984. Non-parametric estimation of the number of classes in a population. Scand J Stat 11:265–270.

Chen XG, Geng AL, Yan R, Gould WD, Ng YL, Liang DT. 2004a. Isolation and characterization of sulphur-oxidizing *Thiomonas* sp. and its potential application in biological deodorization. Lett Appl Microbiol 39:495–503.

Chen CL, Macarie H, Ramirez I, Olmos A, Ong SL, Monroy O, Liu WT. 2004b. Microbial community structure in a thermophilic anaerobic hybrid reactor degrading terephthalate. Microbiology (Reading, Engl.) 150:3429–3440.

Dedysh SN, Ricke P, Liesack W, 2004. NifH and NifD phylogenies: an evolutionary basis for understanding nitrogen fixation capabilities of methanotrophic bacteria Microbiology (Reading, Engl.) 150:1301–1313.

Dedysh SN, Pankratov TA, Belova SE, Kulichevskaya IS, Liesack W. 2006. Phylogenetic analysis and in situ identification of bacteria community composition in an acidic Sphagnum peat bog. Appl Environ Microbiol 72:2110–2117.

Donald R, Southam G. 1999. Low temperature anaerobic bacterial diagenesis of ferrous monosulfide to pyrite. Geochim Cosmochim Acta 63:2019–2023.

Drobner E, Huber H, Rachel R, Stetter KO 1992. *Thiobacillus plumbophilus* sp. nov., a novel galena and hydrogen oxidizer. Arch Microbiol 157:213–217.

Druschel GK, Labrenz M, Thomsen-Ebert T, Fowle DA, Banfield JF. 2002. Geochemical modeling of ZnS in biofilms: An example of ore depositional processes. Econ Geol 97:1319–1329.

Eder W, Ludwig W, Huber R. 1999. Novel 16S rRNA gene sequences retrieved from highly saline brine sediments of Kebrit Deep, Red Sea. Arch Microbiol 172:213–218.

Finneran KT, Forbush HM, VanPraagh CV, Lovley DR. 2002. *Desulfitobacterium metallireducens sp. nov.*, an anaerobic bacterium that couples growth to the reduction of metals and humic acids as well as chlorinated compounds. Int J Syst Evol Microbiol 52:1929–1935.

Fortin D, Davis B, Southam G, Beveridge TJ. 1995. Biogeochemical phenomena induced by bacteria within sulfidic mine tailings. J Indust Microbiol 14:178–185.

Fredrickson JK, Onstott TC. 1996. Microbes deep inside the Earth. Sci Amer 275:68–73.

Geesey GG. 2001. Bacterial behavior at surfaces. Curr Op Microbiol 4:296–300.

Gihring TM, Moser DP, Lin L-H, Davidson M, Onstott TC, Morgan L, Milleson M, Kieft T, Trimarco E, Balkwill DL Dollhopf M. 2006. The distribution of microbial taxa in the subsurface water of the Kalahari Shield, South Africa. Geomicrobiol J 23:415–430.

Giovannoni SJ. 1991. The polymerase chain reaction. In: Stackebrandt E, Goodfellow M. editors. Nucleic acid techniques in bacterial systematics. New York: John Wiley & Sons. P 177–203.

Inagaki F, Nunoura T, Nakagawa S, Teske A, Lever M, Lauer A, Suzuki M, Takai K, Delwiche M, Colwell FS, Nealson KH, Horikoshi K, D'Hondt S, Jorgensen BB 2006. Biogeographical distribution and diversity of microbes in methane hydrate-bearing deep marine sediments on the Pacific Ocean Margin. Proc Natl Acad Sci USA 103:2815–2820.

Inagaki F, Suzuki M, Takai K, Oida H, Sakamoto T, Aoki K, Nealson KH, Horikoshi K. 2003. Microbial communities associated with geological horizons in coastal subseafloor sediments from the sea of Okhotsk. Appl Environ Microbiol 69:7224–7235.

Kaksonen AH, PlumbJJ, Robertson WJ, Franzmann PD, Gibson JAE, Puhakka JA, 2004. Culturable diversity and community fatty acid profiling of sulfate-reducing fluidized-bed reactors treating acidic, metal-containing wastewater. Geomicrobiol J 2:469–480.

Kasai Y, Takahata Y, Hoaki T, Watanabe K. 2005. Physiological and molecular characterization of a microbial community established in unsaturated, petroleum-contaminated soil. Environ Microbiol 7:806–818.

Labrenz M, Druchel G, Thomsen-Ebert T, Gilbert B, Welch SA, Kemner KM, Logan GA, Summons RE, De Stasio G, Bond PL, Lai B, Kelly SD, Banfield JF. 2000. Formation of sphalerite (ZnS) deposits in natural biofilms of sulfate-reducing bacteria. Science 290:1744–1747.

Lane DJ. 1991. Nucleic acid techniques in bacterial systematics. In: Stackebrandt E, Goodfellow M, editors. Nucleic Acid Techniques in Bacterial Systematics. Wiley, New York. P115–175.

Ley RE, Harris JK, Wilcox J, Spear JR, Miller SR, Bebout BM, Maresca JA, Bryant DA, Sogin ML, Pace NR. 2006. Unexpected diversity and complexity of the guerrero negro hypersaline microbial mat. Appl Environ Microbiol 72:3685–3695.

Lin L-H., Gihring T.M., Sherwood Lollar B, Boice E, Pratt LM, Lippmann-Pipke J, Bellamy RES, Hall J, Onstott TC 2006. Planktonic microbial communities associated with fracture-derived groundwater in a deep gold mine of South Africa. Geomicrobiol J 23:474–497.

Little BJ, Wagner PA, Lewandowski Z. 1997. Spatial relations between bacteria and metal surfaces. In: Banfield JF, Nealson KH, editors. Geomicrobiology: Interactions between microbes and minerals. Rev Mineral Geochem 35:123–159.

Lovley DR, Klug MJ. 1983. Sulfate reducers can outcompete methanogens at freshwater sulfate concentrations. Appl Environ Microbiol 45:187–192.

Mills HJ, Hodges C, Wilson K, MacDonald IR, Sobecky PA. 2003. Microbial diversity in sediments associated with surface-breaching gas hydrate mounds in the Gulf of Mexico. FEMS Microbiol Ecol 46:39–52.

Miyoshi T, Iwatsuki T, Naganuma T. 2005. Phylogenetic characterization of 16S rRNA gene clones from deep-groundwater microorganisms that pass through 0.2-micrometer-pore-size filters. Appl Environ Microbiol 71:1084–1088.

Moser DP, Onstott TC, Fredrickson JK, Brockman FJ, Takai K, Balkwill DL, Drake G, Pfiffner S, White DC, Baker BJ, Pratt LM, Fong J, Sherwood Lollar B, Slater G, Phelps TJ, Spoelstra N DeFlaun M, Southam G, Welty AT, Hoek J. 2003. Evolution of microbial community structure and geochemistry in an ultradeep south african gold mine borehole. Geomicrobiol J 20:517–548.

Nakagawa S, Inagaki F, Suzuki Y, Steinsbu BO, Lever MA,Takai K, Engelen B, Sako Y, Wheat CG, Horikoshi K. 2006. Microbial community in black rust exposed to hot ridge flank crustal fluids. Appl. Environ. Microbiol 72:6789–6799.

Onstott TC, Moser DP, Fredrickson JK, Brockman FJ, Pfiffner SM, Phelps TJ, White DC, Peacock A, Balkwill D, Hoover R, Krumholz LR, Borscik M, Kieft TL, Wilson RB. 2003. Indigenous versus contaminant microbes in ultradeep mines. Env Microbiol 5:1168–1191.

Onstott TC, Lin L-H, Davidson M, Mislowack B, Borcsik M, Hall J, Slater G, Ward J, Sherwood Lollar B, Lippmann-Pipke J, Boice E, Pratt LM, Pfiffner

SM, Moser D P, Gihring TM, Kieft T, Phelps TJ, van Heerden E, Litthaur D, DeFlaun M, Rothmel R, Wanger G, Southam G. 2006. The origin and age of biogeochemical trends in deep fracture water of the Witwatersrand Basin, South Africa. Geomicrobiol J 23:369–414.

Pedersen K, Hallbeck L, Arlinger J, Erlandson AC, Jahromi N. 1997. Investigation of the potential for microbial contamination of deep granitic aquifers during drilling using 16S rRNA gene sequencing and culturing methods. J Microbiol Meth 30:179–192.

Penn RL, Banfield JF. 1998. Imperfect oriented attachment: a mechanism for dislocation generation in defect-free nanocrystals. Science 281:969–971.

Pudry KJ, Munson MA, Nedwell DB, Embley TM. 2002. Comparison of the molecular diversity of the methanogenic community at the brackish and marine ends of a UK estuary. FEMS Microbiol Ecol 39:17–21.

Raghoebarsing AA, Pol A, van de Pas-Schoonen KT, Smolders AJP, Ettwig KF, Rijpstra IC, Schouten S, Sinninghe Damste JS, Op den Camp HJM, Jetten MSM, Strous M. 2006. A microbial consortium couples anaerobic methane oxidation to denitrification. Nature 440:918–921.

Rickard D. 1975. Kinetics and mechanism of pyrite formation at low temperatures. Amer J Sci 275:636–652.

Rickard D. 1997. Kinetics of pyrite formation by the H_2S oxidation of iron (II) monosulfide in aqueous solutions between 25 and 125°C: The rate equation. Geochim Cosmochim Acta 61:115–134.

Rickard D, Luther GW III. 1997. Kinetics of pyrite formation by the H_2S oxidation of iron (II) monosulfide in aqueous solutions between 25 and 125°C: The mechanism: Geochim Cosmochim Acta 61:135–147.

Rozanova EP, Tourova TP, Kolganova TV, Lysenko AM, Mityushina LL, Yusupov SK, Belyaev SS. 2001. *Desulfacinum subterraneum* sp. nov., a new thermophilic sulfate-reducing bacteria isolated from a high-temperature oil field. Microbiol 70:466–471.

Sait M, Hugenholtz P, Janssen PH. 2002. Cultivation of globally distributed soil bacteria from phylogenetic lineages previously only detected in cultivation-independent surveys. Environ Microbiol 4:654–666.

Sanford RA, Cole JR Tiedje JM. 2002. Characterization and description of *Anaeromyxobacter dehalogenans* gen. nov., sp. nov., an aryl-halorespiring facultative anaerobic myxobacterium. Appl Environ Microbiol 68:893–900.

Schoonen MAA. 2004. Mechanisms of sedimentary pyrite formation. In: Sulfur Biogeochemistry—Past and present (Amend J.P., Edwards K.J., Lyons T.W., eds). GSA Special Paper 379:117–134.

Schrenk MO, Kelley DS, Delaney JR, Baross JA. 2003. Incidence and diversity of microorganisms within the walls of an active deep-sea sulfide chimney. Appl Environ Microbiol 69:3580–3592.

Sherwood Lollar B, Lacrampe-Couloume G, Slater GF, Ward JA, Moser DP, Gihring TM, Lin L-H, Onstott, TC. 2006. Unravelling abiogenic and biogenic sources of methane in the Earth's deep subsurface. Chem Geol 226:328–339.

Shigematsu T, Tang Y, Mizuno Y, Kawaguchi H, Morimura S, Kida K. 2006. Microbial diversity of mesophilic methanogenic consortium that can degrade long-chain fatty acids in chemostat cultivation. J Biosci Bioeng 102:535–544.

Tringe SG, von Mering C, Kobayashi A, Salamov AA, Chen K, Chang HW, Podar M, Short JM, Mathur EJ, Detter JC, Bork P, Hugenholtz P, Rubin EM. 2005. Comparative metagenomics of microbial communities. Science 308:554–557.

Trudinger PA, Chambers LA, Smith JW. 1985. Low-temperature sulphate reduction: biological versus abiological. Can J Earth Sci 22:1910–1918.

Tuttle JH, Dugan CB, Randles CI. 1969. Microbial sulfate reduction and its potential utility as an acid mine water pollution abatement procedure. Appl Microbiol 17: 297–302.

Tweedie EB. 1981. The geology of the Evander Basin, Southeastern Transvaal, Republic of South Africa. M.Sc. thesis, Univ. of the Witswatersrand, Jhb, 221 pp.

Vetriani C, Tran HV, Kerkhof LJ. 2003. Fingerprinting Microbial Assemblages from the Oxic/Anoxic Chemocline of the Black Sea. Appl Environ Microbiol 69:6481–6488.

Weber KA, Urrutia MM, Churchill PF, Kukkadapu RK, Roden EE. 2006. Anaerobic redox cycling of iron by freshwater sediment microorganisms. Environ Microbiol 8:100–113.

Wilkin RT, Barnes HL. 1997. Formation processes of framboidal pyrite. Geochim Cosmochim Acta 61:323–339.

Wilson AJC. 1963. Mathematical Theory of X-ray Powder Diffraction. Eindhoven, The Netherlands: Philips Technical Library.,

Xie CH, Yokota A. 2006. Zoogloea oryzae sp. nov., a nitrogen-fixing bacterium isolated from rice paddy soil, and reclassification of the strain ATCC 19623 as *Crabtreella saccharophila* gen. nov., sp. nov. Int J Syst Evol Microbiol 56:19–624.

Yamada T, Sekiguchi Y, Imachi H, Kamagata Y, Ohashi A, Harada H. 2005. Diversity, localization, and physiological properties of filamentous microbes belonging to Chloroflexi subphylum I in mesophilic and thermophilic methanogenic sludge granules. Appl Environ Microbiol 71:7493–7503.

Yoshida N, Takahashi N, Hiraishi A. 2005. Phylogenetic characterization of a polychlorinated-dioxin-dechlorinating microbial community by use of microcosm studies. Appl Environ Microbiol 71:4325–4334.

Zhang H, Sekiguchi Y, Hanada S, Hugenholtz P, Kim H, Kamagata Y, Nakamura K. 2003. *Gemmatimonas aurantiaca* gen. nov., sp. nov., a gram-negative, aerobic, polyphosphate-accumulating micro-organism, the first cultured representative of the new bacterial phylum Gemmatimonadetes phyl. nov. Int J Syst Evol Microbiol 53:1155–1163.

Zobell CE. 1946. Studies of redox potential of marine sediments. Bull Am Assoc Petrol Geol 30:477–513.